Original Article

Peak regurgitant diastolic wall shear stress increases in bicuspid aortic valve regurgitation: association of regurgitation severities and aortic root dilation

Shirin Aliabadi[1,2]^, Carmen Lydell[2,3], Louis Kolman[2,4,5], Murad F. Bandali[2,5], Julio Garcia[2,3,5,6]

[1]Department of Biomedical Engineering, University of Calgary, Calgary, AB, Canada; [2]Stephenson Cardiac Imaging Centre, Libin Cardiovascular Institute, University of Calgary, Calgary, AB, Canada; [3]Department of Radiology, University of Calgary, Calgary, AB, Canada; [4]Department of Cardiac Sciences, Cumming School of Medicine, University of Calgary, Calgary, AB, Canada; [5]Libin Cardiovascular Institute, Cumming School of Medicine, University of Calgary, Calgary, AB, Canada; [6]Alberta Children's Hospital Research Institute, University of Calgary, Calgary, AB, Canada

Contributions: (I) Conception and design: S Aliabadi; (II) Administrative support: J Garcia; (III) Provision of study materials or patients: J Garcia, MF Bandali, L Kolman, C Lydell; (IV) Collection and assembly of data: S Aliabadi, J Garcia; (V) Data analysis and interpretation: S Aliabadi; (VI) Manuscript writing: All authors; (VII) Final approval of manuscript: All authors.

Correspondence to: Julio Garcia, PhD. Associate Professor, Suite 0700, Special Service Building (SSB), Stephenson Cardiac Imaging Centre, Foothills Medical Centre – 1403 29th St NW, Calgary, AB, Canada; Department of Radiology, University of Calgary, Calgary, AB, Canada; Libin Cardiovascular Institute, Cumming School of Medicine, University of Calgary, Calgary, AB, Canada; Alberta Children's Hospital Research Institute, University of Calgary, Calgary, AB, Canada. Email: julio.garciaflores@ucalgary.ca.

Background: Bicuspid aortic valve (BAV) disease, especially with regurgitation, lacks adequate clinical management. While root aortopathy is often attributed to genetic factors and aortic regurgitation, the diastolic hemodynamic characteristics in BAV patients with varying regurgitation severities are not well understood. Flow-derived velocity-weighted flow displacement (FD) and wall shear stress (WSS) are linked to aortopathy progression. We sought to evaluate peak systolic and peak regurgitant diastolic regional WSS and FD at the aortic root in BAV patients with regurgitation (BAV-REG) and BAV patients without or with trivial regurgitation (BAV-No/Trivial REG).

Methods: To conduct this retrospective study, a total of 98 subjects (N=38 BAV-No/Trivial REG, age: 48±16 years, N=35 BAV-REG, age: 52±13 years, and N=25 healthy, age: 38±14 years) were recruited. All subjects underwent routine cardiac magnetic resonance imaging (MRI) followed by four-dimensional cardiovascular magnetic resonance flow imaging using a 3.0 Tesla MRI scanner. Regional peak systolic (WSS_{Sys}) and peak regurgitant diastolic (WSS_{Dia}) WSS as well as FD (FD_{Sys}, FD_{Dia}) at annulus, sinus of Valsalva, sinotubular junction, and mid ascending aorta planes were calculated by dividing the extracted two-dimensional planes into eight sectors. Patients were also followed for the occurrence of aortic valve surgery. Independent-samples Kruskal-Wallis H test (Bonferroni corrected at a 0.05 significance level), along with univariate and logistic regression analyses statistical tests were used.

Results: BAV-REG had similar planar WSS_{Sys} patterns compared to BAV-No/Trivial REG. However, peak regurgitant planar WSS_{Dia} was significantly higher in BAV-REG compared to both healthy controls and BAV-No/Trivial REG at the annulus and sinus of Valsalva planes ($P<0.05$) in specific left-sided octants. Normalized peak regurgitant FD_{Dia} was significantly higher only in BAV-REG compared to healthy controls ($P=0.03$). WSS_{Dia} showed a significant association with the regurgitation severities at the annulus ($\rho=0.34$, $P<0.001$), sinus of Valsalva ($\rho=0.34$, $P<0.001$), sinotubular junction ($\rho=0.48$, $P<0.001$) planes. Furthermore,

^ ORCID: 0009-0009-7228-5790.

logistic regression analysis highlighted the potential role of peak regurgitant WSS_{Dia} in the likelihood of requiring surgery (β=5.49, P=0.009).

Conclusions: Higher WSS_{Dia} in BAV patients, particularly in BAV-REG, and the significant association between WSS_{Dia} and regurgitation severity underscore its potential pathophysiological role in aortic root dilation.

Keywords: Peak regurgitation; root aortopathy; bicuspid aortic valve (BAV); wall shear stress (WSS); four-dimensional cardiovascular magnetic resonance flow imaging (4D flow CMR)

Submitted Oct 04, 2024. Accepted for publication Feb 21, 2025. Published online Mar 28, 2025.
doi: 10.21037/qims-24-2059
View this article at: https://dx.doi.org/10.21037/qims-24-2059

Introduction

The bicuspid aortic valve (BAV), with a prevalence of 0.77% as reported in a large population-based study and a male-to-female ratio of 2.1:1, is the most common congenital heart defect and is associated with significant lifetime morbidity (1,2). According to the most recent comprehensive imaging-based nomenclature and classification, BAV is categorized into three main groups: I. the fused BAV, II. the 2-sinus BAV, and III. the partially fused BAV. Within the fused subcategories, the right-left (R/L) coronary cusp fusion is the most common BAV phenotype, followed by the right-noncoronary (R/N) cusp fusion, with the left-noncoronary (L/N) cusp fusion being the least common (3). BAV aortopathy is a frequent occurrence in this cohort, affecting around 40% of patients (4). Despite this, definitive management strategies for BAV-associated aortopathy are not well established and existing practice guidelines exhibit significant variability (5). Hence, considerable effort is directed towards discovering alternative biomarkers to enhance risk prediction in BAV-induced aortopathy. In the past decade, non-invasive *in vivo* volumetric quantification and visualization of blood flow using four-dimensional cardiovascular magnetic resonance flow imaging (4D flow CMR) have provided new insights into the relationships between BAV-related biomechanical characteristics and associated aortopathy (6). Significant attention has been given to valve-mediated wall shear stress (WSS), which refers to the frictional force per unit area that blood flow exerts on the vascular endothelium to predict BAV aortopathy progression (7). Additionally, systolic flow eccentricity, defined as the distance between the anatomical center of the aorta and the center of velocity, serves as a simple yet reliable biomarker for assessing abnormal flow, which results in elevated regional WSS in BAV patients (8,9).

BAV aortopathy can occur in the tubular ascending aorta, aortic root, proximal arch, or any combination of these locations (10). Root aortopathy, characterized by dilation at the level of the sinuses of Valsalva (SoV), is associated with younger ages, male gender, and aortic regurgitation (11,12). The root phenotype is relatively frequent in RL cusp fusion and rare in RN BAV (13). Recent evidence indicates that this phenotype of BAV aortopathy signifies a more malignant and rapidly progressive condition, with a higher risk of aortic dissection (14). Two key research theories have emerged to explain the causes of BAV-related aortopathy. The first theory suggests that genetic factors are the primary contributors, specifically to aortic root dilation (15). The second proposes that the damaging effects of altered flow dynamics, associated with structurally abnormal valves, are significant contributors (9,16). Although confined aortic root dilation is typically attributed to connective tissue disorders (5), the extent and impact of non-invasive hemodynamics biomarkers in BAV patients, particularly those with aortic regurgitation, merit thorough scrutiny at this location. Aortic regurgitation is one of the most frequent aortic valve complications, associated with a higher rate of aortic complications, and it can predict adverse events even after isolated aortic valve replacement (17,18). The presence of aortic stenosis has been associated with increased systolic WSS independent of the BAV phenotypes (19). This relationship has not been well studied in BAV patients with regurgitation in both systolic and diastolic phases.

Given the unclear impact of different BAV phenotypes and accompanying aortic regurgitation on WSS alteration and aortic root dilatation, we sought to evaluate the association between BAV phenotypes with different regurgitation severities and aortic root dilatation by assessing abnormal WSS and flow displacement (FD) caused

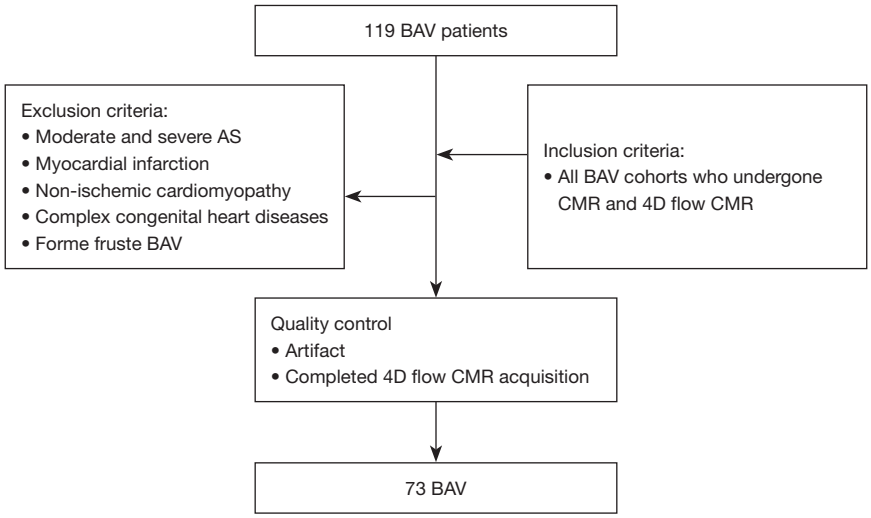

Figure 1 Exclusion process for the BAV cohort. AS, aortic stenosis; BAV, bicuspid aortic valve; 4D flow CMR, four-dimensional cardiovascular magnetic resonance flow imaging.

by systolic blood flow jet and diastolic regurgitant jet. We hypothesized that in cases of BAV-induced regurgitation, the regional WSS at the aortic root is expected to increase significantly due to the impact of the regurgitant jet. This diastolic WSS could have a negative impact due to the longer duration of diastole relative to systole. We present this article in accordance with the STROBE reporting checklist (available at https://qims.amegroups.com/article/view/10.21037/qims-24-2059/rc).

Methods

Study cohort

We retrospectively analyzed a total of 73 eligible BAV patients considering the inclusion and exclusion criteria provided in *Figure 1*. BAV patients were subdivided into R/L, R/N cusp fusions, Type 0 groups, and different MRI-coded regurgitation severity groups. To minimize the effect of aortic stenosis secondary to BAV, patients with moderate to severe stenosis were excluded. Healthy volunteers ≥18 years of age were recruited and underwent identical workflow. They were required to have no known cardiovascular disease, hypertension, or diabetes, and no contraindications for magnetic resonance imaging (MRI).

Patients were enrolled as part of a pre-specified sub-study within our local observational clinical cardiovascular registry. To ensure statistical robustness, we calculated a minimum sample size of 10 subjects per cohort using Eng's sample size estimation method (20). The study was managed using cardioDI^{TM}, a commercial software developed by Cohesic Inc. in Calgary, AB, Canada. This software streamlined the collection of patient informed consent, health questionnaires, and standardized the gathering of MRI-related data. Patients were classified using standardized codes that reflected their clinical referral indications for BAV, including the characterization of BAV morphology. The study adhered to the principles of the Declaration of Helsinki (as revised in 2013). It received approval from the Conjoint Health Research Ethics Board at the University of Calgary (REB#13-0902), and informed consent was obtained from all participants.

CMR data acquisition

All participants underwent a standardized imaging protocol using 3.0 Tesla MRI Siemens scanners (Skyra or Prisma, Erlangen, Germany) with a 32-channel body coil. To assess the function of the left ventricle (LV), multi-planar segmented Electrocardiogram-gated, time-resolved balanced steady-state free precession (SSFP) cine imaging was performed in 4-chamber, 3-chamber, 2-chamber, and short-axis views, covering the entire heart at end-expiration. Five to ten minutes after administering 0.2 mmol/kg of gadolinium contrast (Gadovist®, Bayer Inc., Mississauga, ON, Canada), whole-heart 4D flow CMR was conducted using free-breathing diaphragmatic navigator gating and

retrospective electrocardiogram-gated techniques to comprehensively assess intracardiac 3D volumetric blood flow. However, a cohort of healthy controls did not undergo contrast enhanced CMR angiography. The same sequence was executed on both scanners. The following parameters were set: velocity encoding range in all directions (VENC) =150–250 cm/s, flip angle =15°, acquired spatial resolution (row × column × slice) =(2.0–3.6 mm) × (2.0–3.0 mm) × (2.5–3.5 mm), field of view (FoV) with sagittal slab =[240–350] × [320–400] mm^2, temporal resolution =25–35 ms, timeframe =30, bandwidth =455–495 Hz/pixel, echo time: 2.01–2.35 ms, and pulse repetition time =4.53–5.07 ms, generalized autocalibrating partially parallel acquisition (GRAPPA), R=4. The overall scan duration varied between 8 and 12 minutes, depending on factors such as physiological conditions, defined scan parameters, and respiratory gating efficiency.

CMR imaging and 4D-flow analyses

Different MRI-coded regurgitation severities, aortic diameters, and heart volumes were assessed using a dedicated clinical software cvi[42] v5.11.5 (Circle Cardiovascular Imaging Inc., Calgary, AB, Canada). Body surface area (BSA) was calculated based on the Mosteller formula to index the parameters when necessary. Valve morphologies were assessed using en face view cine SSFP images acquired in the short-axis orientation, allowing for a comprehensive evaluation of the aortic valve. The 2020 American College of Cardiology/American Heart Association Joint Committee Guideline was followed for the standard grading of aortic regurgitation based on the regurgitation fraction (21), which was measured using through-plane 2D phase-contrast flow images. To achieve reasonable statistical power, aortic regurgitation was classified into two main groups: BAV patients without or with trivial regurgitation (BAV-No/Trivial REG) and BAV patients with regurgitation (BAV-REG). BAV-REG includes 16 BAV patients with mild (regurgitant fraction <30%), 9 with moderate (regurgitant fraction 30% to 49%), and 8 with severe regurgitation (regurgitant fraction ≥50%).

Preprocessing, and 3D segmentation

4D flow CMR analysis was performed using in-house software developed in MATLAB (2021b) with the workflow outlined schematically in *Figure 2*. An automated preprocessing procedure was applied to each scan to compensate for sources of errors such as phase offset errors (Maxwell terms, eddy currents, and gradient field non-linearity), noise, and velocity aliasing using a MATLAB tool developed by Bock *et al.* (*Figure 2A*) (22). The personalized flow profile for each subject was computed throughout the cardiac cycle by extracting two 2D planes from the 3D-segmented proximal ascending aorta and calculating the average for enhanced accuracy. The maximum flow value and its corresponding timepoint were considered the peak systole. The maximum negative flow value, or the minimum flow value at the time of isovolumetric relaxation, and its corresponding timepoint were identified as the peak regurgitation timepoint in diastole. Additionally, a 3D phase-contrast magnetic resonance angiography (PCMRA) volume was calculated to aid 3D aorta segmentation by making the mediastinal great vessels transparent, as previously described (22). The time-averaged segmentation was applied to the desired peak diastolic time point and was manually adjusted using the corresponding magnitude grayscale images when necessary. Finally, we obtained two time-specific masks for each subject (*Figure 2B*).

WSS analysis

The WSS algorithm requires inputs of a time-resolved 3D surface of the segmented vessel lumen (consisting of vertices and faces) and an associated 3D velocity vector field derived from phase-contrast MRI measurements (23). The simplified equation for the WSS vector measurement:

$$\vec{\tau} = 2\mu\left(\dot{\varepsilon}\cdot\vec{n}\right) \quad [1]$$

Where the μ denotes blood viscosity (0.0032 Pa·s). the term $\dot{\varepsilon}$, indicates the deformation rate and $\vec{n}$, is the vector pointing inward at the vessel wall's surface. The algorithm generates an array of WSS vectors mapped onto the surface of the vessel's interior. To avoid the effect of noise, the average of 5% maximum WSS was measured in the segmented aortic volume during the peak systolic and peak regurgitation timepoints, defined based on the personalized flow profile (*Figure 2C*). Then, the 3D segmented aorta's centerline was calculated using a validated algorithm that generates precise volumetric skeletons through subvoxel distance field computation (24). Subsequently, the volumetric skeleton was utilized to extract the coordinates of 2D planes at anatomical landmarks, positioned perpendicular to the centerline, to derive regional WSS from the 3D volume. The anatomical landmarks facilitated the extraction of four planes at the locations of the aortic Annulus, SoV, sinotubular junction (STJ), and the middle ascending aorta (Mid-

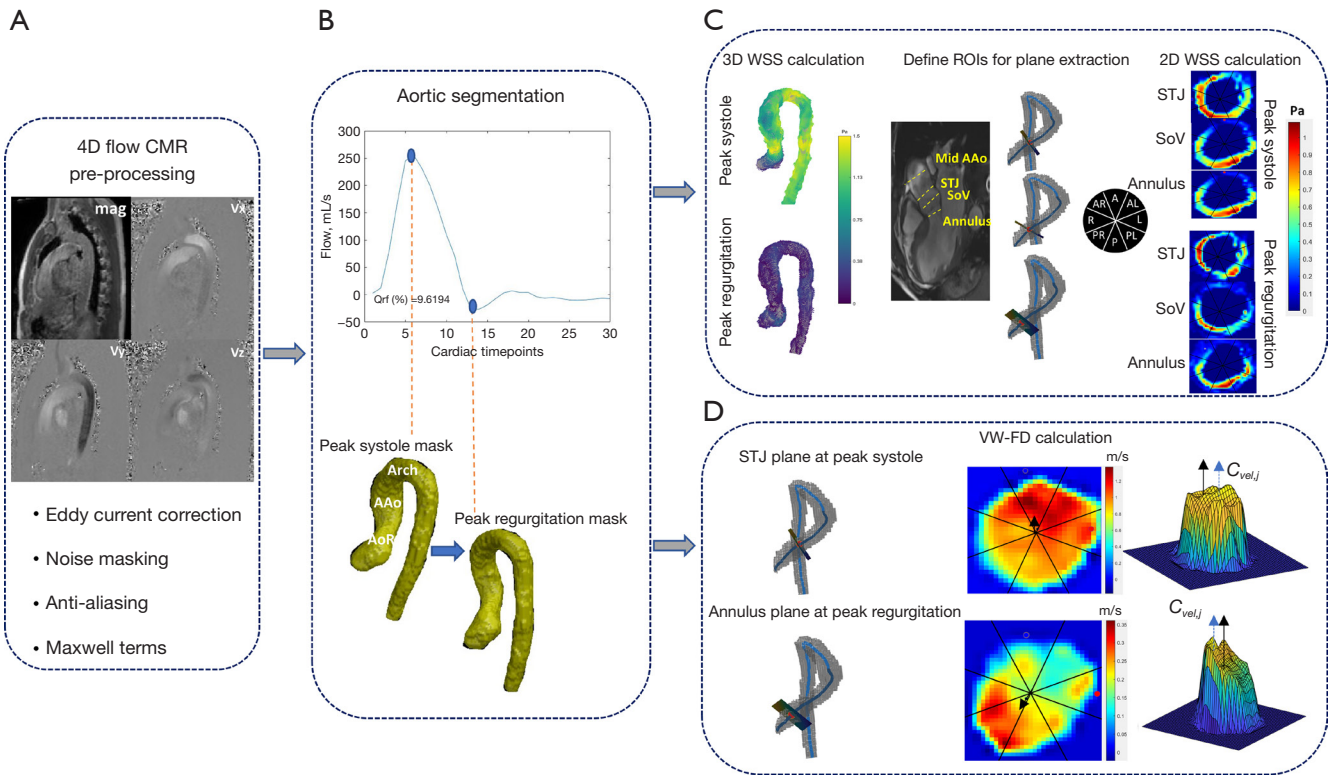

Figure 2 Workflow. (A) Preprocessing of 4D flow CMR data, (B) segmentation of thoracic aorta at specific timepoints, (C) calculating WSS in the region of interest in volume and extracting planar WSS at the ROIs, (D) calculating velocity-weighted FD at the 2D planes located at the ROIs. 4D flow CMR, four-dimensional cardiovascular magnetic resonance flow imaging; AAo, ascending aorta; AoR, aortic root; FD, flow displacement; Qrf, regurgitant flow fraction; ROIs, regions of interest; SoV, sinus of Valsalva; STJ, sinotubular junction; VW, velocity weighted; WSS, wall shear stress.

AAo) at the level of the pulmonary trunk. This allowed for the measurement of peak regional systolic WSS at the four planes ($WSS_{Sys,Annulus}$, $WSS_{Sys,SoV}$, $WSS_{Sys,STJ}$, and $WSS_{Sys,Mid\text{-}AAo}$). To measure regional WSS at the peak regurgitation timepoint, the extracted planes specifically targeted the aortic annulus, SoV, and STJ ($WSS_{Dia,Annulus}$, $WSS_{Dia,Sov}$, and $WSS_{Dia,STJ}$). The circumference of the planes was divided into eight equal sectors. Peak WSS_{Sys} and peak regurgitant WSS_{Dia} values were determined for each of these eight aortic wall sectors. These sectors were designated based on the anatomical position of the AAo as follows: A (anterior), AL (anterior-left), L (left), PL (posterior-left), P (posterior), PR (posterior-right), R (right), and AR (anterior-right).

Normalized velocity weighted FD analysis

FD was defined as the distance from the center of the lumen to the velocity-weighted centroid for both the forward flow and the backward jet flow in cases of regurgitation. The algorithm that generates precise volumetric skeletons was used to calculate the 3D segmented aorta's centerline. The velocity weighted centroid (C_{vel}) was calculated using this equation:

$$C_{vel,j} = \frac{\sum_i r_{ij}|v_i|}{\sum_i |v_i|}, i = x, y \quad [2]$$

Where i indicates lumen pixels and the center of velocity was determined by calculating the average position of lumen pixels (r_i) weighted according to their velocity values (v_i) (*Figure 2D*).

To calculate the FD, the cross-sectional plane coordinates used for extracting planar WSS were employed. The FD at peak systole was obtained from the planes at the locations of the STJ and Mid-AAo, and then divided by the diameter of

the planes to account for individual anatomical differences and calculate the normalized FD (normalized $FD_{Sys,STJ}$, $FD_{Sys,Mid\text{-}AAo}$). The peak regurgitation FD was obtained from the plane at the location of the aortic annulus. This FD value was then divided by the diameter of the planes to calculate the normalized FD (normalized peak regurgitant $FD_{Dia,Annulus}$) (25).

The circumference of the planes was divided into eight equal sectors. The direction of FD was defined for each patient in each cross-sectional plane. We assessed the agreement between the flow-derived biomarkers by comparing the locations of the FD and the location of the highest systolic WSS. Following the methodology described by (26), we categorized the differences in octant positions as follows: a difference of 0 octant positions indicates no difference, and a difference of 1 octant position clockwise or counter-clockwise indicates one position away from the maximum median WSS. We considered a difference of 0 or 1 octant positions to represent good to excellent agreement between the biomarkers.

Statistical analysis

Statistical analyses were conducted using IBM SPSS (Version 28). Initially, the Shapiro-Wilk test was used to assess the distribution of variables. Depending on the distribution, unpaired two-tailed Student's *t*-tests with equal variance and Mann-Whitney *U* tests were utilized to detect significant differences between pairwise groups, as well as one-way analysis of variance (ANOVA) for comparing basic clinical characteristics and cardiac function. Due to the non-normal distribution of peak systolic and peak regurgitation WSS, and normalized FD at the planes of interest across different groups, the Kruskal-Wallis *H* test was used for multiple comparisons. Bonferroni correction was applied to adjust for multiple comparisons across three groups, resulting in three pairwise comparisons. To implement this correction, each obtained P value was multiplied by three, while maintaining the significance threshold at $P<0.05$. Additionally, Pearson's product-moment correlation coefficient and Spearman's rank correlation coefficient were applied based on the variable type. Logistic regression models were fitted with surgery outcome as the dependent variable and sex, BAV disease, and regurgitation as dichotomous variables, and aortic root size, maximum WSS, age, LV mass, LV volume, systolic and diastolic BP, and cardiac output (CO) as continuous variables.

Results

Study group assignments

Baseline demographics of healthy volunteers and BAV patients is provided in *Table 1*. The study cohort included BAVs (38 BAV-No/Trivial REG, age: 48±16 years, 16 females, 35 BAV-REG, 4 females, age: 52±13 years) and 25 healthy, 7 females, age: 38±14 years. The average age of the BAV cohort was significantly higher than that of the healthy control group. The BAV cohort also had a significantly larger LV mass (P=0.02). Overall, the indexed root diameters at the locations of the SoV and STJ were significantly larger in BAV patients compared to the healthy control group. The BAV-REG group had markedly larger left ventricular end diastolic and systolic volumes, as well as increased LV mass and CO, compared to the BAV-No/Trivial REG group. When dividing BAV cases into those referred for aortic valve surgery (N=24) and those not undergoing surgery (N=49), significant differences were noted in terms of BSA, LV mass, and annulus and SoV sizes (P=0.03, 0.02, 0.03, and 0.03, respectively). In Table S1, the clinical characteristics of BAV patients, considering the available phenotypes, are also provided.

Aortic planar WSS assessment

The planar magnitude of regional WSS is compared once among healthy individuals and those with BAV, considering both available phenotypes and regurgitation status.

Healthy control *vs.* BAV-No/Trivial REG and BAV-REG (peak systole)

The localized planar WSS_{Sys} along the aortic root and Mid-AAo at the four predefined cross-sectional planes for BAV-No/Trivial REG, BAV-REG, and healthy subjects in the eight sectors at the peak systolic phase is illustrated in *Figure 3A*. The overall peak planar $WSS_{Sys,Annulus}$, $WSS_{Sys,SoV}$ values were lower and more symmetric across all three groups compared to $WSS_{Sys,STJ}$ and $WSS_{Sys,Mid\text{-}AAo}$. Significant differences in planar peak WSS_{Sys} between the healthy group and both BAV-No/Trivial REG and BAV-REG groups were observed in the P octant (P=0.004) and PR octant (P=0.016, 0.022 respectively) at the annulus, and in the P octant (P=0.04) at the SoV planes. More octants showed significant differences for peak planar $WSS_{Sys,STJ}$, and $WSS_{Sys,Mid\text{-}AAo}$. In pairwise group comparisons, at least one significant difference was found for peak planar

Table 1 Patient demographics and left ventricular function

Parameters	All cohorts			Regurgitation status			Outcome		
	Control	BAV	P value	BAV-No/Trivial REG	BAV-REG	P value	No surgery	Surgery	P value
N [female]	25 [7]	73 [20]	–	38 [16]	35 [4]	–	49 [13]	24 [7]	–
Age (years)	38±14	50±15	0.003*	48±16	52±13	0.2	48±16	53±13	0.05
Annulus (mm/m^2)	14.91±2.2	15.36±1.8	0.3	14.8±2.1	15.5±1.6	0.1	14.9±1.9	15.9±1.4	0.03*
SoV (mm/m^2)	16.6±2.3	18.7±2.5	<0.001*	17.9±2.2	19.3±2.5	0.01*	18.2±2.2	19.5±2.7	0.03*
STJ (mm/m^2)	15±1.9	19.1±4.1	<0.001*	19.1±3.5	19.7±3.2	0.4	19.1±3.3	19.9±3.6	0.3
BSA (m^2)	1.9±0.3	2.01±0.2	0.5	1.9±0.3	2.1±0.1	0.05	1.9±0.2	2.1±0.2	0.03*
Heart rate (bpm)	62.7±10.6	63±11.4	0.9	64.1±10.6	61.7±12.4	0.4	61.5±12.1	65.6±9.8	0.3
SBP (mmHg)	113.4±18.6	114.1±16.2	0.9	116.2±18.6	111.2±12	0.2	112.9±17.3	116.1±14.7	0.2
DBP (mmHg)	62.3±16.9	67.8±12.4	0.2	71.3±12.8	63.2±10.5	0.008*	67.3±11.8	67.7±13.7	0.3
LVESV (mL)	62.1±22.1	82.4±54.2	0.1	69.7±31.7	99.3±71.5	0.02*	72.6±29.3	105.2±83.5	0.1
LVEDV (mL)	161.9±45.4	189.2±75.3	0.1	167.4±55.2	218.2±88.7	0.01*	171.4±54.2	229.1±99.3	0.1
LVEF (%)	61.9±5.9	58.2±10.2	0.1	58.9±9.4	57.2±11.4	0.5	57.9±9	58.2±12.9	0.7
LVCO (L/min)	6.5±1.6	7±2.3	0.3	6.4±1.6	7.8±2.8	0.01*	6.4±1.6	8.2±3	0.1
LV mass (g)	102.9±32.5	132.7±50.3	0.02*	120.1±41.5	149.6±56.6	0.02*	117.8±41.2	161.4±57.2	0.02*

Values are shown as mean ± standard deviation or n. For normally distributed variables, an unpaired two-tailed equal variance Student's *t*-test (significant for P<0.05) were used. For skewed variables, equivalent non-parametric tests were used. *, statistically significant results. BSA, body surface area; BAV-No/Trivial REG, bicuspid aortic valve with no or trivial regurgitation; DBP, diastolic blood pressure; LVCO, left ventricular cardiac output; LV, left ventricle; LVEDV, left ventricular end-diastolic volume; LVEF, left ventricular ejection fraction; LVESV, left ventricular end-systolic volume; SoV, sinus of Valsalva; STJ, sinotubular junction; SBP, systolic blood pressure.

$WSS_{Sys,STJ}$ in all octants except A, compared to healthy controls.

Peak planar $WSS_{Sys,Mid\text{-}AAo}$ pattern was highly asymmetric and heterogeneous in the BAV patients compared to the healthy control group. WSS magnitude was markedly lower between pairwise BAV subgroups compared to healthy control in all octants (Bonferroni corrected P values <0.05) except A, AR, and AL. Although the WSS was higher for BAV subgroups at the A and AR octants compared to healthy control, these differences were not statistically significant. The peak planar WSS_{Sys} was not significantly different in any of the octants between BAV-No/Trivial REG and BAV-REG in all planes.

The percentage of octant location of FD is matched with location of maximum peak $WSS_{Sys,STJ}$, which maximized at Mid-AAo planes for BAV-REG and BAV-No/Trivial REG as well as BAV phenotypes (*Figure 3B* and Figure S1). To evaluate the conformity between the areas of highest WSS_{Sys} and the octants where normalized FD_{Sys} is located, the percentage of participants' normalized FD locations is displayed for each corresponding plane at the STJ, and Mid-AAo planes. The median maximum WSS for the BAV-No/Trivial REG at the Mid-AAo plane was highest at A and AR octants, corresponding to the normalized FD location for 98% of these BAV participants [8(R)+16(AR)+61(A) + 13(AL)]. This value for the BAV-REG is highest at the A and AR octants, matching to the 91% of this BAV participants.

The peak planar WSS_{Sys} along the aortic root and Mid-AAo at the four predefined cross-sectional planes for BAV phenotypes, regardless of regurgitation severity, as well as healthy subjects in the eight sectors, is illustrated in Figure S1.

Healthy control *vs.* BAV-No/Trivial REG and BAV-REG (peak regurgitation)

Figure 4 visualizes the backward diastolic flow in three groups, including healthy individuals and BAV-No/Trivial REG and BAV-REG, at peak regurgitant diastolic timepoints. Regurgitant flow jets in BAV cases with higher

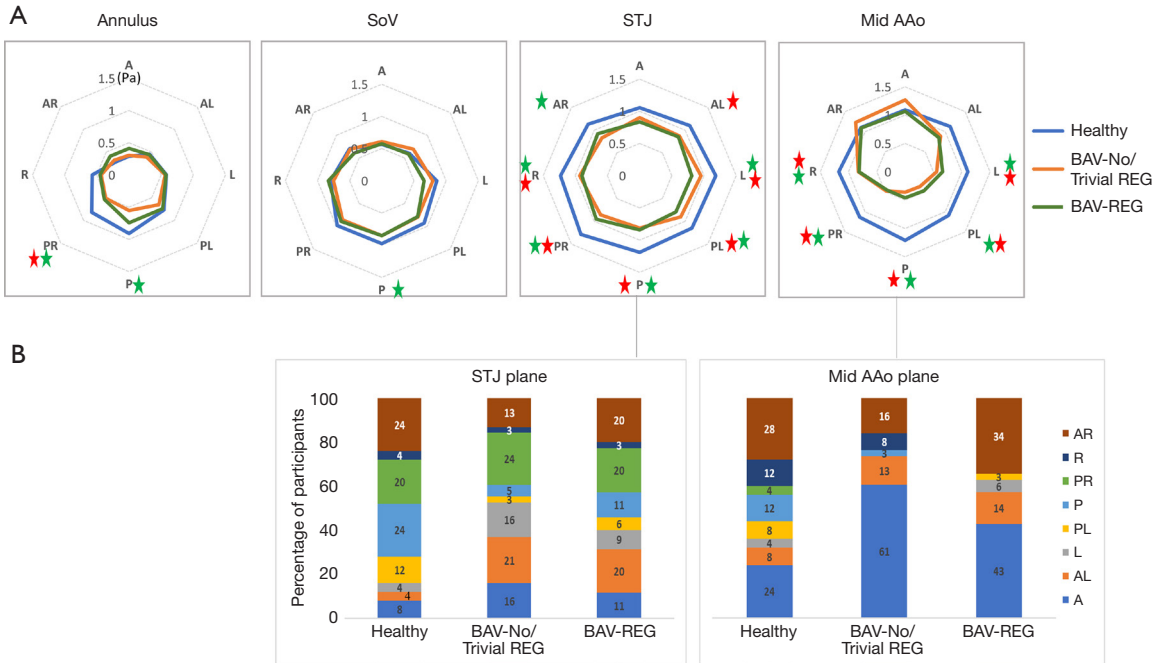

Figure 3 Planar peak WSS_{Sys} and FD_{Sys} percentage per octant for each group. (A) Peak WSS_{Sys} at four predefined planes in each octant, comparing three groups: healthy control, BAV-No/Trivial REG, and BAV-REG. Green star indicates significant P value for pairwise comparison between healthy and BAV-No/Trivial REG. Red star indicates significant P value for pairwise comparison between healthy with BAV-REG; (B) the percentage of FD_{Sys} direction per octants for the groups is provided, to show the conformity of FD_{Sys} direction with the areas of highest WSS_{Sys}. Stars show statistically significant level <0.05. AAo, ascending aorta; BAV-No/Trivial REG, bicuspid aortic valve with no or trivial regurgitation; BAV-REG, bicuspid aortic valve with regurgitation; FD_{Sys}, systolic flow displacement; SoV, sinus of Valsalva; STJ, sinotubular junction; WSS_{Sys}, systolic wall shear stress; AR, anterior-right; R, right; PR, posterior-right; P, posterior; PL, posterior-left; L, left; AL, anterior-left; A, anterior.

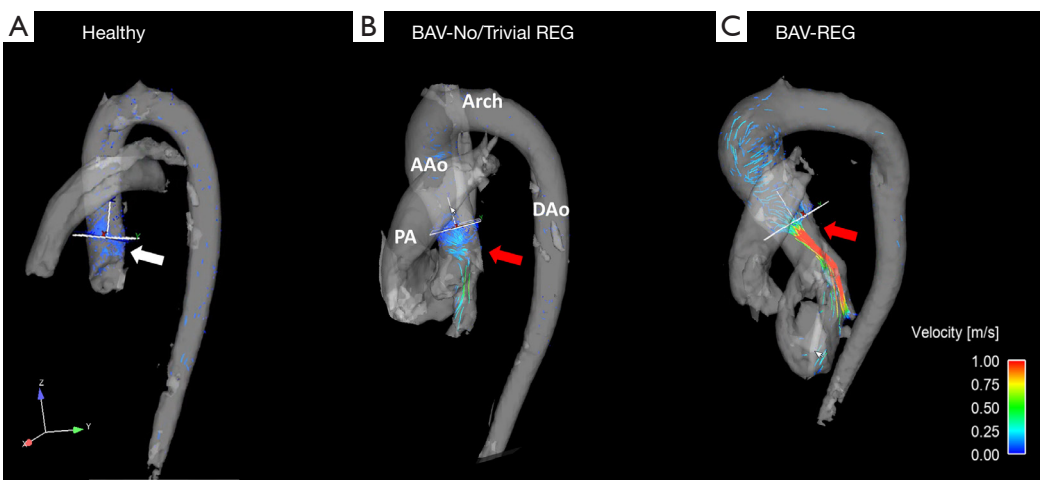

Figure 4 Peak regurgitant diastolic flow patterns. (A) A 25-year-old healthy control, (B) a 28-year-old BAV patient with R/L coronary cusp fusion and (C) a 28-year-old BAV patient with R/L coronary cusp fusion. The white arrow indicates the aortic root location in a healthy subject, while the red arrows indicate the regurgitant flow in BAV patients at the location of the aortic root. BAV, bicuspid aortic valve; BAV-No/Trivial REG, BAV patients without or with trivial regurgitation; BAV-REG, patients with regurgitation; PA, pulmonary artery; AAo, ascending aorta; DAo, descending aorta; R/L, right-left.

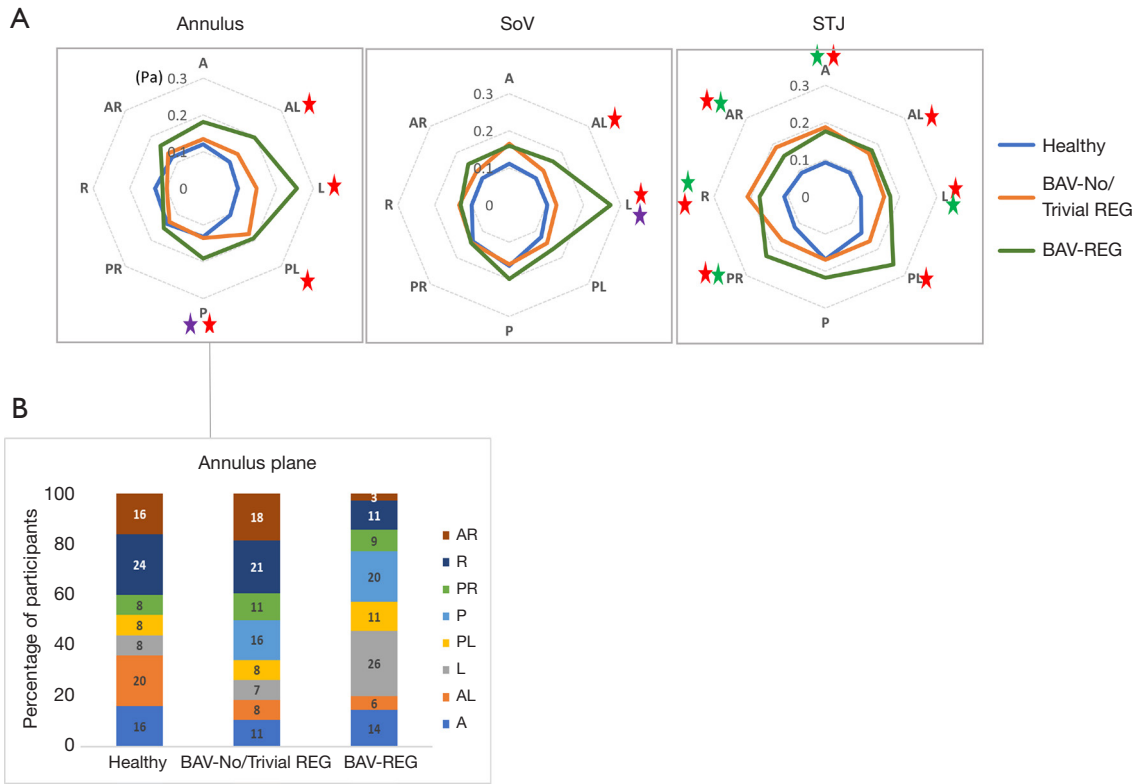

Figure 5 Planar peak regurgitant WSS_{Dia} and FD_{Dia} percentage per octant for each group. (A) Peak regurgitant WSS_{Dia} at three predefined planes in each octant, comparing three groups: healthy control, BAV-No/Trivial REG, and BAV-REG. Green star indicates significant P value for pairwise comparison between healthy and BAV-No/Trivial REG. Red star indicates significant P value for pairwise comparison between healthy with BAV-REG. Purple star indicates significant P value for pairwise comparison between BAV-No/Trivial REG, with BAV-REG; (B) the percentage of peak regurgitant FD_{Dia} direction per octants for the groups is provided, to show the conformity of peak regurgitant FD_{Dia} direction with the areas of highest WSS_{Dia}. Stars show statistically significant level <0.05. BAV-No/Trivial REG, bicuspid aortic valve with no or trivial regurgitation; BAV-REG, bicuspid aortic valve with regurgitation; FD_{Dia}, diastolic flow displacement; SoV, sinus of Valsalva; STJ, sinotubular junction; WSS_{Dia}, diastolic wall shear stress; AR, anterior-right; R, right; PR, posterior-right; P, posterior; PL, posterior-left; L, left; AL, anterior-left; A, anterior.

severity are considerable and potentially destructive (*Figure 5*). A illustrates the planar WSS across the aortic root at three predefined cross-sectional planes, comparing BAV patients and healthy subjects in eight sectors at the peak diastolic regurgitant timepoint. In healthy controls, the WSS magnitude and pattern were very negligible and symmetric compared to the BAV subgroups. Peak regurgitant $WSS_{Dia,Annulus}$ value was significantly higher in BAV-REG at the AL, L, PL, and P octants (P=0.033, <0.001, 0.003, and 0.047 respectively) compared to healthy controls. Additionally, it was considerably higher in BAV-REG compared to BAV-No/Trivial REG at the P octant (P=0.028), while no significant differences were observed in any of the eight sectors between healthy controls and BAV-No/Trivial REG. Hence, $WSS_{Dia,SoV}$ followed the same pattern as peak regurgitant WSS_{Dia} at the annulus, though with fewer octants showing significance. Peak regurgitant $WSS_{Dia,STJ}$ was significantly higher in almost all octants for BAV subgroups compared to healthy controls, but for the P octant.

To provide a visual association between the WSS magnitude and the octants where normalized FD is defined, the percentage of participants' normalized FD locations is shown for the annulus plane (*Figure 5B*). The peak regurgitant normalized $FD_{Dia,Annulus}$ matched with the median of the maximum diastolic WSS at the L octant for 43% in BAV-REG, and at the PL octant for 32% of BAV-No/Trivial REG. This indicates that the location of the velocity-weighted centroid is less directed at this location compared

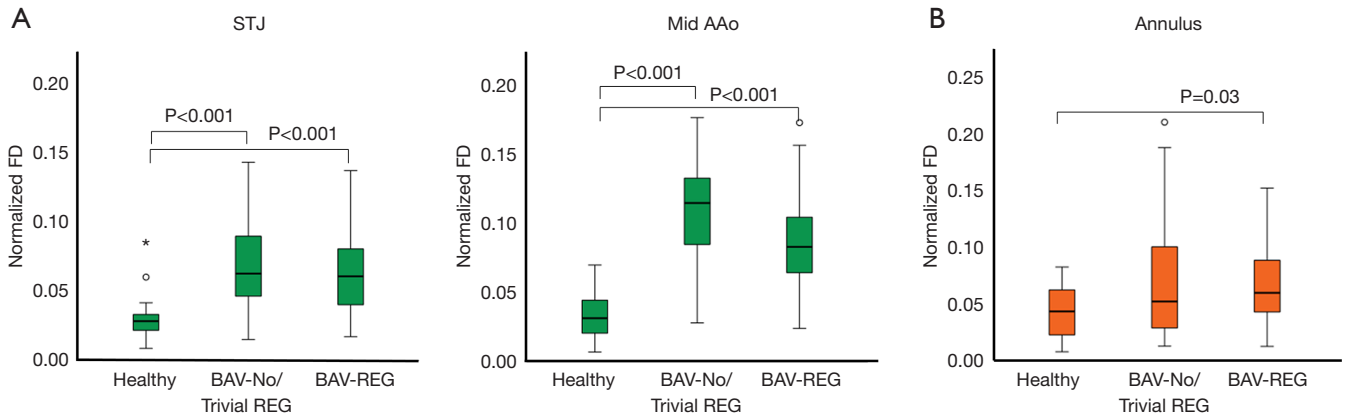

Figure 6 Comparison of normalized flow displacement (FD_{Sys}). (A) At peak systole (FD_{Sys}) at two predefined planes (STJ and Mid-AAo), and (B) at peak regurgitant diastole (FD_{Dia}) at the Annulus plane comparing three groups: healthy control, BAV-No/Trivial REG, and BAV-REG. AAo, ascending aorta; BAV-No/Trivial REG, bicuspid aortic valve with no or trivial regurgitation; BAV-REG, bicuspid aortic valve with regurgitation; FD_{Sys}, systolic flow displacement; FD_{Dia}, diastolic flow displacement; STJ, sinotubular junction.

to Mid-AAo plane at peak systole.

The peak regurgitant planar WSS_{Dia} along the aortic root at three predefined cross-sectional planes for different BAV phenotypes, irrespective of their regurgitation severities, and healthy subjects in the 8 sectors is illustrated in Figure S2. Peak regurgitant $WSS_{Dia,Annulus}$ and $WSS_{Dia,SoV}$ were significantly higher for R/L cusp fusion BAV compared to healthy controls, but not for other BAV phenotypes (R/N and Type0).

Normalized velocity-weighted FD analysis

Normalized $FD_{Sys,STJ}$ and $FD_{Sys,Mid-AAo}$ were significantly higher in both BAV-No/Trivial REG and BAV-REG groups compared to the healthy cohort (P<0.001), as shown in *Figure 6A*. Interestingly, normalized peak regurgitant $FD_{Dia,Annulus}$ was significantly higher in the BAV REG group compared to the healthy cohort (P=0.031) whereas no significant difference was observed between the BAV-No/Trivial REG group and the healthy controls.

Dividing BAV cases into different phenotypes (R/L, R/N, and Type 0), regardless of their regurgitation status, R/L cusp fusion phenotype reveals significantly higher eccentric flow during peak diastole compared to healthy controls (P=0.032). However, the differences between the pairwise BAV phenotypes were not markedly significant (Figure S3).

Univariate and multivariate functional and structural associations

Results of the univariable analysis are shown in *Table 2*. Age was positively associated with root diameters at the SoV and STJ locations (ρ=0.38, P<0.001 and ρ=0.41, P<0.001), but not with the Annulus diameter. While planar WSS_{Sys} was poorly correlated with root diameters, planar WSS_{Dia} showed a correlation with SoV and was strongest at STJ diameters (ρ=0.38, P<0.001). Additionally, both normalized $FD_{Sys,STJ}$ and normalized peak regurgitant $FD_{Dia,Annulus}$ were correlated with SoV and STJ diameters. The strongest correlation was observed between normalized peak regurgitant FD_{Dia} at the Annulus and STJ diameter (ρ=0.42, P<0.001).

Peak regurgitant WSS_{Dia} was positively correlated with regurgitation severity at three extracted planes located at the aortic root from Annulus to SoV and STJ planes (ρ=0.343, P<0.001, ρ=0.345, P<0.001 and ρ=0.482, P<0.001 respectively) (*Figure 7A-7C*). Conversely, no significant correlation was observed between the regurgitation fraction and WSS_{Sys}. A Moderate correlation was found between regurgitation severities with normalized peak regurgitant FD_{Dia} at the Annulus plane (ρ=0.446, P<0.001) (*Figure 7D*).

A logistic regression model was fitted with surgery outcome following 4D flow CMR scan as the dependent variable to assess the effect of different variables on surgical outcomes. The forward likelihood method was used to omit non-significant variables. The final logistic regression model included five independent variables: age, LV mass, aortic annulus size index and $WSS_{Sys,STJ}$ and $WSS_{Dia,STJ}$ (*Figure 8*).

Both $WSS_{Dia,STJ}$ and $WSS_{Sys,STJ}$ were significantly associated with the likelihood of requiring surgery, with

Table 2 Correlations between indexed root diameter and variables of interest

Parameters	Annulus		SoV		STJ	
	ρ	P value	ρ	P value	ρ	P value
Age	–0.02	0.84	0.38	<0.001*	0.41	<0.001*
Peak Sys						
$WSS_{Annulus}$	0.06	0.52	–0.15	0.13	–0.07	0.45
WSS_{SoV}	0.01	0.91	–0.13	0.2	–0.015	0.14
WSS_{STJ}	0.02	0.79	–0.11	0.25	–0.2	0.05
Peak REG						
$WSS_{Annulus}$	0.16	0.12	0.18	0.07	0.25	0.01*
WSS_{SoV}	0.13	0.21	0.21	0.04*	0.29	0.005*
WSS_{STJ}	0.01	0.88	0.22	0.02*	0.38	<0.001*
Peak Sys						
N FD_{STJ}	0.04	0.64	0.2	0.04*	0.28	0.006*
Peak REG						
N $FD_{Annulus}$	–0.04	0.67	0.31	0.002*	0.42	<0.001*

Pearson correlation used when both variables were parametric; Spearman's correlation used when at least 1 variable was non-parametric. *, statistically significant results. N FD, normalized flow displacement; Sys, systole; REG, regurgitation; SoV, sinus of Valsalva; STJ, sinotubular junction; WSS, wall shear stress; ρ, correlation coefficient.

coefficient values of 5.49 (P=0.009) and 2.007 (P=0.033) respectively. This means that by increasing 0.1 Pa value in peak regurgitant $WSS_{Dia,STJ}$, and peak $WSS_{Sys,STJ}$ the likelihood of surgery increases by 73% ($e^{0.1*5.49}$=1.73) and 22% respectively.

Discussion

The distinctive feature of this study lies in the comprehensive, non-invasive characterization of two closely related and previously validated flow-derived biomarkers, including WSS and normalized velocity-weighted FD at anatomical landmarks of the aortic root employing 4D flow CMR (25,27). This assessment takes into account the available BAV phenotypes and regurgitation status evaluated at personalized peak systolic and peak regurgitation diastolic timepoints. Compelling evidence from studies utilizing the 4D-flow technique is available, which seeks to establish a connection between advanced flow-derived biomarkers and the prevalence of aortic remodeling during the systolic phase in BAV patients. This supports the hemodynamic hypothesis in BAV aortopathy, attributing changes in the composition of the aortic wall to altered flow dynamics (28,29).

The results of our study demonstrate that BAV patients exhibit overall higher regional peak regurgitant WSS_{Dia} at the root planes, independent of regurgitant status, age and root diameter, compared to healthy controls at the personalized diastolic timepoints.

Not only did BAV-REG show significantly higher peak regurgitant WSS_{Dia}, in line with previous studies (30), but BAV-No/Trivial REG also demonstrated a significant higher peak regurgitant $WSS_{Dia,STJ}$ compared to the healthy control. The significant role of BAV-REG is unveiled as we move from the STJ plane toward the annulus plane, where the impact of the regurgitant jet becomes more evident. We observed significantly higher peak regurgitant WSS_{Dia} compared to both the healthy cohort and the BAV-No/Trivial REG group. A significant correlation was observed between the severity of regurgitation and peak regurgitant WSS_{Dia}, emphasizing that BAV-REG is independently associated with aortic root dilatation (12).

Diving the BAV cohorts into phenotypes to assess peak diastolic WSS_{Dia}, just R/L cusp fusion showed significant difference compared to healthy confirming the association of this phenotype with aortic root dilation (31).

Although the primary aim of this study was to analyze the

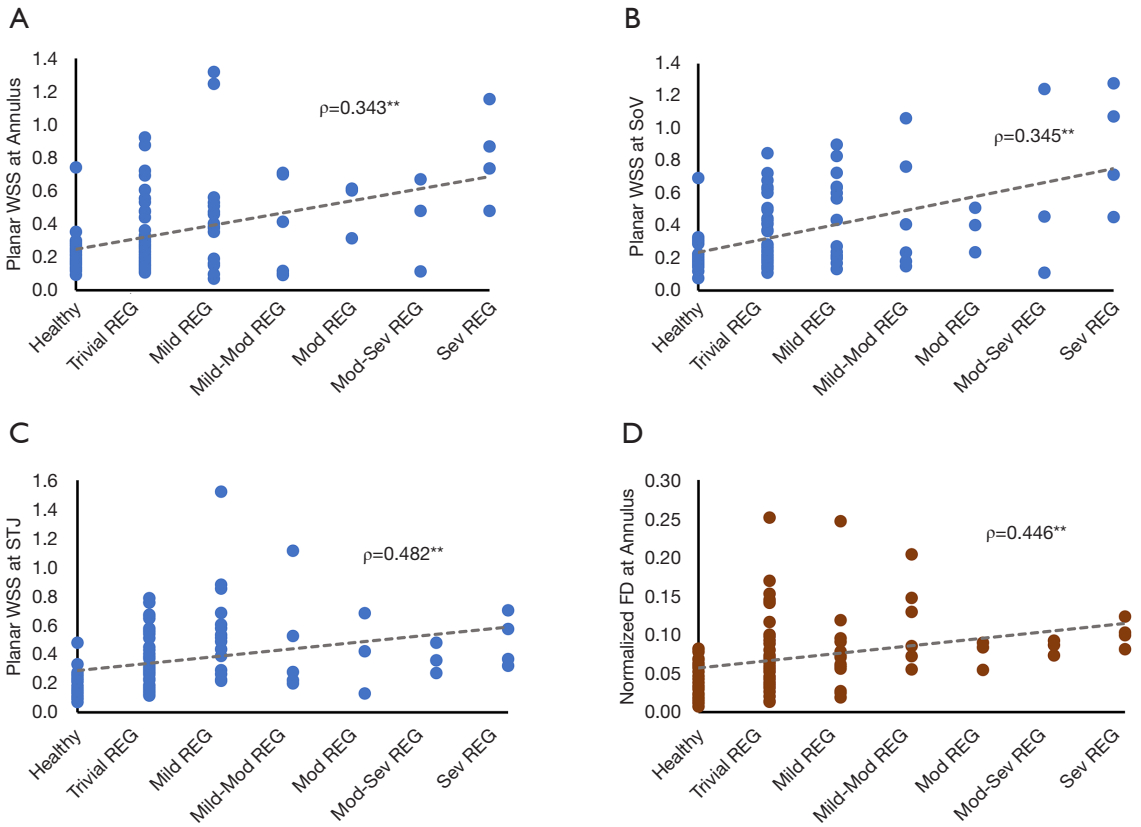

Figure 7 Correlation analysis between regurgitation severities ($N_{Trivial}$=42, N_{Mild}=16, $N_{Mild\text{-}Mod}$=5, N_{Mod}=3, $N_{Mod\text{-}Sev}$=3, N_{Sev}=4) and peak regurgitant wall shear stress (WSS_{Dia}) along the aortic root at the planes on Annulus (A), SoV (B) and STJ (C), and (D) between regurgitation severities and normalized peak regurgitant diastolic flow displacement (FD_{Dia}) at the plane located at Annulus (brown plot). **, statistically significant (P<0.001). Mod, moderate; SoV, sinus of Valsalva; STJ, sinotubular junction; REG, regurgitation; Sev, severe; WSS_{Dia}, diastolic wall shear stress; ρ, correlation coefficient.

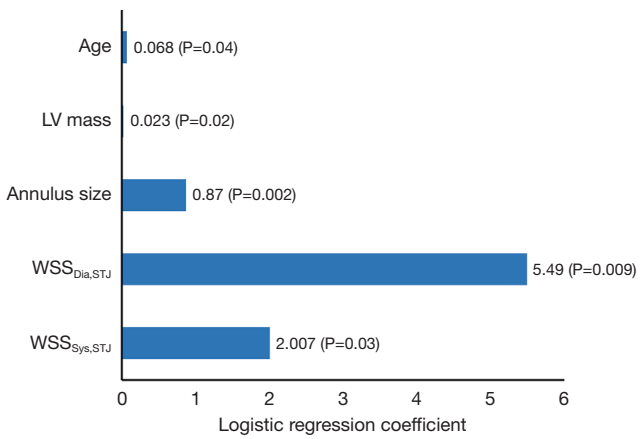

Figure 8 Logistic regression coefficient analysis for aortic surgery prediction. LV, left ventricle; $WSS_{Dia,STJ}$, peak regurgitant diastolic wall shear stress at the sinotubular junction plane; $WSS_{Sys,STJ}$, peak systolic wall shear stress at the sinotubular junction plane.

aortic root location, the planar WSS was also measured at the plane located at the Mid-AAo. We observed a symmetric WSS pattern at the SoV location when considering BAV phenotypes and the presence of regurgitation. This indicates that hemodynamic alterations are not considerable at this location in peak systole. The significant role of hemodynamic alterations becomes evident farther from the SoV, at the STJ, and is most pronounced at the Mid-AAo plane. This pattern is very asymmetric for both BAV-No/Trivial REG and BAV-REG subgroups, but symmetric for healthy controls. This indicates that patients with normally functioning BAV still exhibit altered blood flow patterns compared to healthy tricuspid aortic valve subjects, which might be exacerbated in the presence of valvular complications (32).

A notable finding in our study, in contrast to peak regurgitant WSS_{Dia}, is that in most octants, the healthy

cohort exhibits significantly higher peak WSS_{Sys} compared to all BAV subgroups. This finding aligns with a previous study using the same BAV cohort (33) and with research by Barker *et al.*, which observed reduced systolic WSS in BAV patients with retrograde flow compared to healthy controls (34). Additionally, Bollache *et al.* suggested that increased systolic aortic WSS is strongly linked to elastic fiber thinning, a hallmark of aortopathy, particularly in patients with predominant aortic stenosis and less dilated aortas but is less important in patients with predominant aortic regurgitation (29). By dividing our BAV cohort into those with and without regurgitation, we showed that systolic WSS is also reduced in BAV-No/Trivial REG when the ascending aortic diameter and age is not matched with healthy controls. This highlights the considerable role of stenosis and matching aortic diameter in increasing peak WSS_{Sys} in AAo. Hence, in BAV patients who do not have meaningful stenosis and exhibit different rates of aortic dilation, peak WSS_{Sys} may not predict aortic aneurysm. This suggests that additional flow biomarkers need to be validated to enhance the assessment and prediction of aortic events in this BAV cohort.

Consistent with previous literature, the WSS_{Sys} magnitude was higher for both R/L and R/N BAV compared to healthy controls at the AR and A octants of the plane at Mid-AAo (6), although this difference was not markedly significant. At the remaining octants, a decrease in WSS over time has been observed, which can be attributed to the compensatory enlargement of the aorta (35) in agreement with a study by Truong *et al.*, found that WSS was inversely proportional to the cube of the vessel radius (36). This result may also be attributed to the older average age of our BAV cohort compared to the healthy controls, which aligns with a study by van Ooij *et al.* that showed significant associations between age and the hemodynamic parameters of velocity and WSS at peak systole (37). Additionally, Jarvis *et al.* showed that aortic pulse wave velocity, which is inversely related to WSS, increased significantly with age in both genders (38). Emerging research in the systemic vasculature also suggests that lower WSS is associated with increased arterial stiffness and the development of atherogenic conditions (39). These modifications in arterial compliance and diameter may ultimately impact the flow waveform and the viscous hemodynamic forces exerted on the arterial walls. Thus, the importance of using peak WSS_{Sys} to predict disease progression should be particularly emphasized in the early stages and less severe forms of BAV aortopathy.

The marked displacement of forward flow direction in BAV patients at the STJ and Mid-AAo planes suggests that the elevated WSS observed in non-dilated healthy can primarily attributed to size-related factors rather than the amount of FD. In contrast, the BAV cohort encompasses a range of dilation stages in these planes, which affects the observed WSS. The location of normalized peak FD_{Sys} corresponded to the peak systolic WSS distribution, with the strongest correspondence observed at the Mid-AAo. Additionally, significantly increased normalized peak regurgitant FD_{Dia} was observed in BAV-REG compared to healthy controls, with more than 50% of BAV-REG patients having the center of velocity (regurgitant jet direction) at the L, PL, and P octants. These directions of the backward flow jet may interfere with the normal functioning of the mitral valve by hindering the mobility of the anterior mitral leaflet, leading to left ventricular and mitral valve remodeling (40). This is highlighted by a study showing that the mitral valve can be elongated in patients with BAV, with this effect being more pronounced in those with concomitant aortic regurgitation (41). Hence, BAV cases with aortic regurgitation make the cohort prone to cardiovascular remodeling and diastolic dysfunction (42) indicating that the destructive effect is not limited to the aortic root location.

The majority of BAV patients who were referred later for surgical interventions received exclusively valvular procedures and had notably larger Annulus and STJ diameters compared to those who did not undergo surgery. Additionally fitted logistic regression model indicates that peak regurgitant $WSS_{Dia,STJ,}$ is a significant differentiating factor between patients who were referred for surgery and those who were not. Therefore, although the magnitude of diastolic WSS at the root location is significantly lower than systolic WSS, it may still serve as a crucial physiological parameter for consideration in preoperative assessments.

Limitation

Our study faced a number of limitations. The time-averaged PCMRA mask was used as a reference in this study. However, the results are still valuable for characterizing normal and pathological spatiotemporal variations in WSS. Furthermore, the WSS profile throughout the cardiac cycle for some BAV and healthy cases was plotted, which is consistent with findings from a previous study (30). The lower spatial resolution inherent in 4D flow CMR, particularly at the aortic root location,

leads to an underestimation of WSS. This underestimation may be even exacerbated by the use of higher VENC, which is intended to prevent velocity aliasing but can increase noise in measurements of slow flow. Since BAV patients with moderate and severe stenosis were excluded from our analysis, this issue of velocity noise should be less problematic. The acquired spatial resolution of 4D-flow CMR data exhibited non-isotropic variations across study participants. Notably, WSS is particularly sensitive to changes in spatial resolution compared to other hemodynamic parameters (43). Still group comparisons remain credible, due to the random distribution of resolution variations across groups. These limitations underscore the critical role of resolution in the accuracy of 4D-flow measurements and advocate for standardization in future studies to enhance the comparability and reproducibility of results. Although age is considered a confounding factor in assessing 3D velocity fields and 3D WSS in the thoracic aorta, our study is limited by the unmatched ages between the healthy control and our BAV cohorts. However, this finding aligns with a previous study using the same but age matched BAV cohort (33). Our sample size was also constrained by the available number of cases per grade of regurgitation, limiting us to groups of BAV-No/Trivial REG and BAV-REG to maintain statistical power. Finally, a longitudinal clinical study of a larger cohort, along with stratification of patients according to the severity of aortic stenosis and aortic regurgitation and valve morphology, is needed to validate aortic root diastolic WSS.

Conclusions

This study underscores a more meaningful hemodynamic role of peak regurgitant WSS_{Dia} over peak WSS_{Sys} in BAV patients with regurgitation. The significantly higher values of peak regurgitant WSS_{Dia} and peak regurgitant normalized FD_{Dia} in BAV-REG at the Annulus, along with their association with the severity of regurgitation, suggest that these diastolic biomarkers may offer valuable insights into hemodynamic phenomena potentially contributing to root dilation. Given that abnormal hemodynamics alongside genetic factors may contribute, the impact of these hemodynamic changes at peak regurgitant timepoints in BAV patients with backward flow warrants further investigation as a potential metric for risk stratification in BAV root aortopathy. Such insights could facilitate optimal treatment planning, the development of effective clinical guidelines, and improved patient outcomes. To achieve this, studies with larger sample sizes and longitudinal designs are essential to provide more robust evidence.

Acknowledgments

The invaluable contributions of the investigators, clinical staff, and patient participants involved in the Cardiovascular Imaging Registry of Calgary (CIROC) are greatly appreciated by the authors.

Footnote

Reporting Checklist: The authors have completed the STROBE reporting checklist. Available at https://qims.amegroups.com/article/view/10.21037/qims-24-2059/rc

Funding: This work was supported by the University of Calgary; J.G. start-up funding (#11022618 and #11021988); Calgary Health Foundation; Alberta Innovates Health Solutions (AIHS); and the Canadian Institutes for Health Research (CIHR). We acknowledge the support of the Natural Science and Engineering Research Council of Canada/Conseil de recherche en science naturelles et en génie du Canada (#RGPIN-2020-04549 and #DGECR-2020-00204), and the support of NSERC Alliance – Alberta Innovates Advance Program (#232403115). The study was also supported by the University of Calgary, Department of Biomedical Engineering, Graduate Program, and Libin Cardiovascular Institute (Kenneth M Stephenson Graduate Scholarship in Cardiovascular Research) (to S.A.).

Conflicts of Interest: All authors have completed the ICMJE uniform disclosure form (available at https://qims.amegroups.com/article/view/10.21037/qims-24-2059/coif). S.A. reports that the study was supported by the University of Calgary, Department of Biomedical Engineering, Graduate Program, and Libin Cardiovascular Institute (Kenneth M Stephenson Graduate Scholarship in Cardiovascular Research). The other authors have no conflicts of interest to declare.

Ethical Statement: The authors are accountable for all aspects of the work in ensuring that questions related to the accuracy or integrity of any part of the work are appropriately investigated and resolved. The study adhered to the principles of the Declaration of Helsinki (as revised in 2013). It received approval from the Conjoint Health

Research Ethics Board at the University of Calgary (REB#13-0902), and informed consent was obtained from all participants.

References

1. Sillesen AS, Vøgg O, Pihl C, Raja AA, Sundberg K, Vedel C, Zingenberg H, Jørgensen FS, Vejlstrup N, Iversen K, Bundgaard H. Prevalence of Bicuspid Aortic Valve and Associated Aortopathy in Newborns in Copenhagen, Denmark. JAMA 2021;325:561-7.
2. Yang LT, Ye Z, Wajih Ullah M, Maleszewski JJ, Scott CG, Padang R, Pislaru SV, Nkomo VT, Mankad SV, Pellikka PA, Oh JK, Roger VL, Enriquez-Sarano M, Michelena HI. Bicuspid aortic valve: long-term morbidity and mortality. Eur Heart J 2023;44:4549-62.
3. Michelena HI, Della Corte A, Evangelista A, Maleszewski JJ, Edwards WD, Roman MJ, et al. International consensus statement on nomenclature and classification of the congenital bicuspid aortic valve and its aortopathy, for clinical, surgical, interventional and research purposes. Eur J Cardiothorac Surg 2021;60:448-76.
4. Masri A, Kalahasti V, Alkharabsheh S, Svensson LG, Sabik JF, Roselli EE, Hammer D, Johnston DR, Collier P, Rodriguez LL, Griffin BP, Desai MY. Characteristics and long-term outcomes of contemporary patients with bicuspid aortic valves. J Thorac Cardiovasc Surg 2016;151:1650-1659.e1.
5. Borger MA, Fedak PWM, Stephens EH, Gleason TG, Girdauskas E, Ikonomidis JS, Khoynezhad A, Siu SC, Verma S, Hope MD, Cameron DE, Hammer DF, Coselli JS, Moon MR, Sundt TM, Barker AJ, Markl M, Della Corte A, Michelena HI, Elefteriades JA. The American Association for Thoracic Surgery consensus guidelines on bicuspid aortic valve-related aortopathy: Full online-only version. J Thorac Cardiovasc Surg 2018;156:e41-74.
6. Rodríguez-Palomares JF, Dux-Santoy L, Guala A, Kale R, Maldonado G, Teixidó-Turà G, Galian L, Huguet M, Valente F, Gutiérrez L, González-Alujas T, Johnson KM, Wieben O, García-Dorado D, Evangelista A. Aortic flow patterns and wall shear stress maps by 4D-flow cardiovascular magnetic resonance in the assessment of aortic dilatation in bicuspid aortic valve disease. J Cardiovasc Magn Reson 2018;20:28.
7. Katritsis D, Kaiktsis L, Chaniotis A, Pantos J, Efstathopoulos EP, Marmarelis V. Wall shear stress: theoretical considerations and methods of measurement. Prog Cardiovasc Dis 2007;49:307-29.
8. Sigovan M, Dyverfeldt P, Wrenn J, Tseng EE, Saloner D, Hope MD. Extended 3D approach for quantification of abnormal ascending aortic flow. Magn Reson Imaging 2015;33:695-700.
9. Mahadevia R, Barker AJ, Schnell S, Entezari P, Kansal P, Fedak PW, Malaisrie SC, McCarthy P, Collins J, Carr J, Markl M. Bicuspid aortic cusp fusion morphology alters aortic three-dimensional outflow patterns, wall shear stress, and expression of aortopathy. Circulation 2014;129:673-82.
10. Fazel SS, Mallidi HR, Lee RS, Sheehan MP, Liang D, Fleischman D, Herfkens R, Mitchell RS, Miller DC. The aortopathy of bicuspid aortic valve disease has distinctive patterns and usually involves the transverse aortic arch. J Thorac Cardiovasc Surg 2008;135:901-7, 907.e1-2.
11. Michelena HI, Suri RM, Katan O, Eleid MF, Clavel MA, Maurer MJ, Pellikka PA, Mahoney D, Enriquez-Sarano M. Sex Differences and Survival in Adults With Bicuspid Aortic Valves: Verification in 3 Contemporary Echocardiographic Cohorts. J Am Heart Assoc 2016;5:e004211.
12. Della Corte A, Bancone C, Quarto C, Dialetto G, Covino FE, Scardone M, Caianiello G, Cotrufo M. Predictors of ascending aortic dilatation with bicuspid aortic valve: a wide spectrum of disease expression. Eur J Cardiothorac Surg 2007;31:397-404; discussion 404-5.
13. Pagé M, Mongeon FP, Stevens LM, Soulière V, Khairy P, El-Hamamsy I. Aortic dilation rates in patients with biscuspid aortic valve: correlations with cusp fusion phenotype. J Heart Valve Dis 2014;23:450-7.
14. Kalogerakos PD, Zafar MA, Li Y, Mukherjee SK, Ziganshin BA, Rizzo JA, Elefteriades JA. Root Dilatation Is More Malignant Than Ascending Aortic Dilation. J Am Heart Assoc 2021;10:e020645.
15. Girdauskas E, Geist L, Disha K, Kazakbaev I, Groß T, Schulz S, Ungelenk M, Kuntze T, Reichenspurner H, Kurth I. Genetic abnormalities in bicuspid aortic valve root phenotype: preliminary results. Eur J Cardiothorac Surg 2017;52:156-62.

16. Guala A, Dux-Santoy L, Teixido-Tura G, Ruiz-Muñoz A, Galian-Gay L, Servato ML, Valente F, Gutiérrez L, González-Alujas T, Johnson KM, Wieben O, Casas-Masnou G, Sao Avilés A, Fernandez-Galera R, Ferreira-Gonzalez I, Evangelista A, Rodríguez-Palomares JF. Wall Shear Stress Predicts Aortic Dilation in Patients With Bicuspid Aortic Valve. JACC Cardiovasc Imaging 2022;15:46-56.
17. Michelena HI, Khanna AD, Mahoney D, Margaryan E, Topilsky Y, Suri RM, Eidem B, Edwards WD, Sundt TM 3rd, Enriquez-Sarano M. Incidence of aortic complications in patients with bicuspid aortic valves. JAMA 2011;306:1104-12.
18. Wang Y, Wu B, Li J, Dong L, Wang C, Shu X. Impact of Aortic Insufficiency on Ascending Aortic Dilatation and Adverse Aortic Events After Isolated Aortic Valve Replacement in Patients With a Bicuspid Aortic Valve. Ann Thorac Surg 2016;101:1707-14.
19. van Ooij P, Markl M, Collins JD, Carr JC, Rigsby C, Bonow RO, Malaisrie SC, McCarthy PM, Fedak PWM, Barker AJ. Aortic Valve Stenosis Alters Expression of Regional Aortic Wall Shear Stress: New Insights From a 4-Dimensional Flow Magnetic Resonance Imaging Study of 571 Subjects. J Am Heart Assoc 2017;6:e005959.
20. Eng J. Sample size estimation: how many individuals should be studied? Radiology 2003;227:309-13.
21. Otto CM, Nishimura RA, Bonow RO, Carabello BA, Erwin JP 3rd, Gentile F, Jneid H, Krieger EV, Mack M, McLeod C, O'Gara PT, Rigolin VH, Sundt TM 3rd, Thompson A, Toly C. 2020 ACC/AHA Guideline for the Management of Patients With Valvular Heart Disease: Executive Summary: A Report of the American College of Cardiology/American Heart Association Joint Committee on Clinical Practice Guidelines. J Am Coll Cardiol 2021;77:450-500.
22. Bock J, Kreher BW, Hennig J, Markl M. Optimized pre-processing of time-resolved 2D and 3D phase contrast MRI data. In: Proceedings of the 15th Annual meeting of ISMRM, Berlin, Germany; 2007.
23. Stalder AF, Russe MF, Frydrychowicz A, Bock J, Hennig J, Markl M. Quantitative 2D and 3D phase contrast MRI: optimized analysis of blood flow and vessel wall parameters. Magn Reson Med 2008;60:1218-31.
24. Van Uitert R, Bitter I. Subvoxel precise skeletons of volumetric data based on fast marching methods. Med Phys 2007;34:627-38.
25. Sigovan M, Hope MD, Dyverfeldt P, Saloner D. Comparison of four-dimensional flow parameters for quantification of flow eccentricity in the ascending aorta. J Magn Reson Imaging 2011;34:1226-30.
26. van der Palen RLF, Deurvorst QS, Kroft LJM, van den Boogaard PJ, Hazekamp MG, Blom NA, Lamb HJ, Westenberg JJM, Roest AAW. Altered Ascending Aorta Hemodynamics in Patients After Arterial Switch Operation for Transposition of the Great Arteries. J Magn Reson Imaging 2020;51:1105-16.
27. Slager CJ, Wentzel JJ, Gijsen FJ, Thury A, van der Wal AC, Schaar JA, Serruys PW. The role of shear stress in the destabilization of vulnerable plaques and related therapeutic implications. Nat Clin Pract Cardiovasc Med 2005;2:456-64.
28. Rodríguez-Palomares JF, Dux-Santoy L, Guala A, Galian-Gay L, Evangelista A. Mechanisms of Aortic Dilation in Patients With Bicuspid Aortic Valve: JACC State-of-the-Art Review. J Am Coll Cardiol 2023;82:448-64.
29. Bollache E, Guzzardi DG, Sattari S, Olsen KE, Di Martino ES, Malaisrie SC, van Ooij P, Collins J, Carr J, McCarthy PM, Markl M, Barker AJ, Fedak PWM. Aortic valve-mediated wall shear stress is heterogeneous and predicts regional aortic elastic fiber thinning in bicuspid aortic valve-associated aortopathy. J Thorac Cardiovasc Surg 2018;156:2112-2120.e2.
30. Rizk J, Latus H, Shehu N, Mkrtchyan N, Zimmermann J, Martinoff S, Ewert P, Hennemuth A, Stern H, Meierhofer C. Elevated diastolic wall shear stress in regurgitant semilunar valvular lesions. J Magn Reson Imaging 2019;50:763-70.
31. Della Corte A, Bancone C, Dialetto G, Covino FE, Manduca S, Montibello MV, De Feo M, Buonocore M, Nappi G. The ascending aorta with bicuspid aortic valve: a phenotypic classification with potential prognostic significance. Eur J Cardiothorac Surg 2014;46:240-7; discussion 247.
32. Edlin J, Youssefi P, Bilkhu R, Figueroa CA, Morgan R, Nowell J, Jahangiri M. Haemodynamic assessment of bicuspid aortic valve aortopathy: a systematic review of the current literature. Eur J Cardiothorac Surg 2019;55:610-7.
33. Trenti C, Fedak PWM, White JA, Garcia J, Dyverfeldt P. Oscillatory shear stress is elevated in patients with bicuspid aortic valve and aortic regurgitation: a 4D flow cardiovascular magnetic resonance cross-sectional study. Eur Heart J Cardiovasc Imaging 2024;25:404-12.
34. Barker AJ, Lanning C, Shandas R. Quantification of hemodynamic wall shear stress in patients with bicuspid aortic valve using phase-contrast MRI. Ann Biomed Eng 2010;38:788-800.

35. Rahman O, Scott M, Bollache E, Suwa K, Collins J, Carr J, Fedak P, McCarthy P, Malaisrie C, Barker AJ, Markl M. Interval changes in aortic peak velocity and wall shear stress in patients with bicuspid aortic valve disease. Int J Cardiovasc Imaging 2019;35:1925-34.
36. Truong U, Fonseca B, Dunning J, Burgett S, Lanning C, Ivy DD, Shandas R, Hunter K, Barker AJ. Wall shear stress measured by phase contrast cardiovascular magnetic resonance in children and adolescents with pulmonary arterial hypertension. J Cardiovasc Magn Reson 2013;15:81.
37. van Ooij P, Garcia J, Potters WV, Malaisrie SC, Collins JD, Carr JC, Markl M, Barker AJ. Age-related changes in aortic 3D blood flow velocities and wall shear stress: Implications for the identification of altered hemodynamics in patients with aortic valve disease. J Magn Reson Imaging 2016;43:1239-49.
38. Jarvis K, Scott MB, Soulat G, Elbaz MSM, Barker AJ, Carr JC, Markl M, Ragin A. Aortic Pulse Wave Velocity Evaluated by 4D Flow MRI Across the Adult Lifespan. J Magn Reson Imaging 2022;56:464-73.
39. Cunningham KS, Gotlieb AI. The role of shear stress in the pathogenesis of atherosclerosis. Lab Invest 2005;85:9-23.
40. Galea N, Pambianchi G, Cundari G, Sturla F, Marchitelli L, Putotto C, Versacci P, De Paulis R, Francone M, Catalano C. Impaction of regurgitation jet on anterior mitral leaflet is associated with diastolic dysfunction in patients with bicuspid aortic valve and mild insufficiency: a cardiovascular magnetic resonance study. Int J Cardiovasc Imaging 2022;38:211-21.
41. Charitos EI, Hanke T, Karluss A, Hilker L, Stierle U, Sievers HH. New insights into bicuspid aortic valve disease: the elongated anterior mitral leaflet. Eur J Cardiothorac Surg 2013;43:367-70.
42. Aliabadi S, Sojoudi A, Bandali MF, Bristow MS, Lydell C, Fedak PWM, White JA, Garcia J. Intra-cardiac pressure drop and flow distribution of bicuspid aortic valve disease in preserved ejection fraction. Front Cardiovasc Med 2022;9:903277.
43. Cibis M, Potters WV, Gijsen FJ, Marquering H, van Ooij P, vanBavel E, Wentzel JJ, Nederveen AJ. The Effect of Spatial and Temporal Resolution of Cine Phase Contrast MRI on Wall Shear Stress and Oscillatory Shear Index Assessment. PLoS One 2016;11:e0163316.

Cite this article as: Aliabadi S, Lydell C, Kolman L, Bandali MF, Garcia J. Peak regurgitant diastolic wall shear stress increases in bicuspid aortic valve regurgitation: association of regurgitation severities and aortic root dilation. Quant Imaging Med Surg 2025;15(4):3384-3400. doi: 10.21037/qims-24-2059